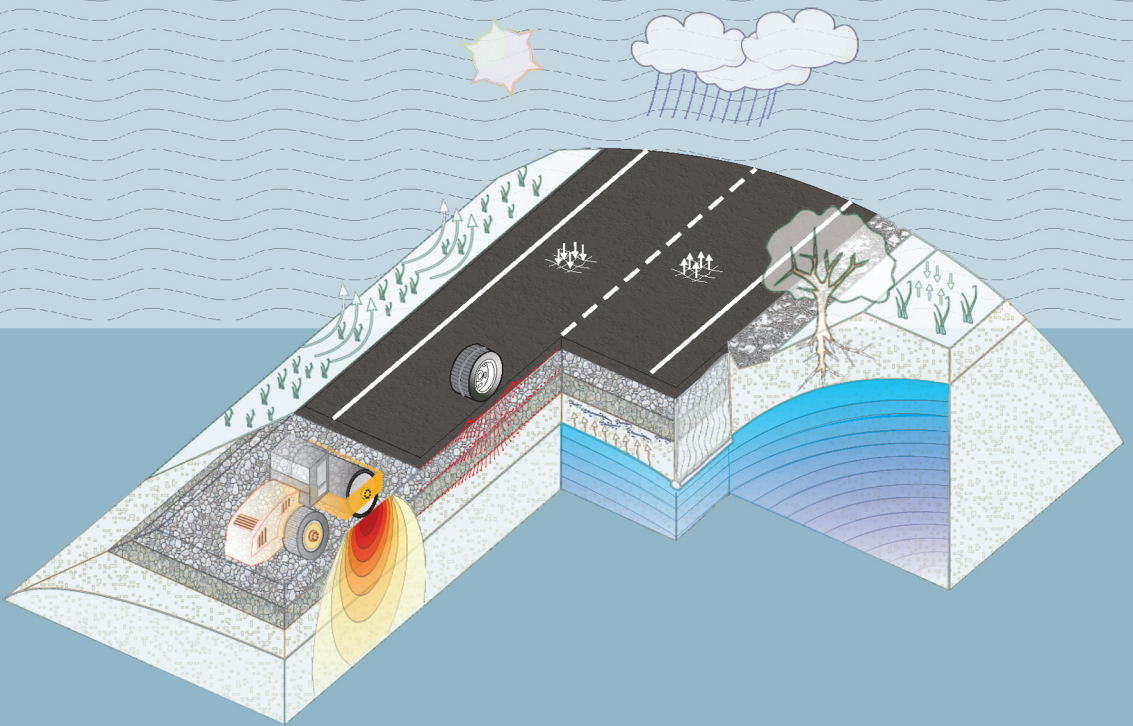


Bernardo Caicedo

Geotechnics of Roads: Advanced Analysis and Modeling



Geotechnics of Roads: Advanced Analysis and Modeling



Taylor & Francis

Taylor & Francis Group

<http://taylorandfrancis.com>

Geotechnics of Roads: Advanced Analysis and Modeling

Bernardo Caicedo

*Department of Civil and Environmental Engineering
Los Andes University, Bogotá, Colombia*



CRC Press

Taylor & Francis Group

Boca Raton London New York

CRC Press is an imprint of the
Taylor & Francis Group, an **informa** business

CRC Press/Balkema is an imprint of the Taylor & Francis Group, an informa business

© 2021 Taylor & Francis Group, London, UK

All rights reserved. No part of this publication or the information contained herein may be reproduced, stored in a retrieval system, or transmitted in any form or by any means, electronic, mechanical, by photocopying, recording or otherwise, without written prior permission from the publishers.

Although all care is taken to ensure integrity and the quality of this publication and the information herein, no responsibility is assumed by the publishers nor the author for any damage to the property or persons as a result of operation or use of this publication and/or the information contained herein.

Library of Congress Cataloging-in-Publication Data

Names: Caicedo, Bernardo, author.

Title: Geotechnics of roads : fundamentals / Bernardo Caicedo (Department of Civil and Environmental Engineering, Los Andes University, Bogotá, Colombia.

Description: Leiden, The Netherlands : CRC Press/Balkema, [2019] |

Includes bibliographical references and index.

Identifiers: LCCN 2018051953 (print) | LCCN 2018044343 (ebook) |

ISBN 9781138600577 (hardcover) | ISBN 9780429025914 (ebook)

Subjects: LCSH: Geotechnical engineering. | Roads—Design and construction. | Road materials. | Soil mechanics.

Classification: LCC TA705 .C27 2019 (ebook) | LCC TA705 (print) |

DDC 625.7/32—dc23

LC record available at <https://lccn.loc.gov/2018051953>

ISBN: 978-1-138-60057-7 (hbk Volume 1)

ISBN: 978-0-429-02591-4 (ebk Volume 1)

DOI: 10.1201/9780429025914

<https://doi.org/10.1201/9780429025914>

ISBN: 978-1-138-60058-4 (hbk Volume 2)

ISBN: 978-0-429-02592-1 (ebk Volume 2)

DOI: 10.1201/9780429025921

<https://doi.org/10.1201/9780429025921>

ISBN: 978-1-138-02956-9 (hbk set of 2 volumes)

ISBN: 978-1-315-22639-2 (ebk set of 2 volumes)

Typeset in Times New Roman
by codeMantra

Dedication

To Gloria
Alejandro and Nicolás.



Taylor & Francis

Taylor & Francis Group

<http://taylorandfrancis.com>

Contents

<i>Author Biography</i>	xiii
<i>Acknowledgments</i>	xv
<i>List of mathematical symbols</i>	xvii

Introduction	I
---------------------	----------

I Distribution of stresses and strains in roads	3
1.1 Relevant equations	3
1.1.1 Boussinesq's solution	3
1.1.2 Cerruti's solution	4
1.1.3 Fröhlich solution	5
1.1.4 Tire–soil interaction	6
1.1.5 Road–vehicle interaction	7
1.1.5.1 Mathematical description of road profiles	8
1.1.6 Burmister's method	9
1.2 Example 1: Calculation of the stress distribution produced by vertical loads using Boussinesq's solution	12
1.2.1 Loaded area and uniform stress	12
1.2.2 Superposition of the stresses produced by each individual loaded area	14
1.2.3 Requirements of Cohesion corresponding to the Mohr–Coulomb criterion	15
1.2.4 Concluding remarks	21
1.3 Example 2: Use of Cerruti's solution to calculate the stresses produced by horizontal loads	21
1.3.1 Stresses in the half-space	22
1.3.2 Requirements of cohesion for the Mohr–Coulomb criterion	24
1.3.3 Concluding remarks	25
1.4 Example 3: Tire–road interaction using the Hertz theory and the Fröhlich stress distribution	25
1.4.1 Elastic properties of the equivalent tire	26
1.4.2 Contact stress applied by the tire on the road	27

1.4.3	Stresses in the half-space using the Fröhlich solution for stress distribution	28
1.4.4	Concluding remarks	30
1.5	Example 4: Calculation of the vehicle–road interaction	31
1.5.1	Discretization in time of the differential equation	32
1.5.2	Vehicle interaction in a bumpy road	33
1.5.3	Vehicle interaction on actual roads	36
1.5.4	Concluding remarks	43
1.6	Examples 5: Computation of stresses in a three-layered road structure using Burmister’s method	43
1.6.1	Approximation of the load using Bessel functions	43
1.6.2	Calculation of the vertical and radial stresses using Burmister’s method	44
1.6.3	Concluding remarks	49
1.7	Example 6: Tridimensional distribution of stresses produced by moving wheel loads	49
1.7.1	Stresses produced by a circular load in a cylindrical coordinate system	51
1.7.2	Transformation of stresses from cylindrical into Cartesian coordinates	57
1.7.3	Principal stresses, rotation, and invariants p and q	59
1.7.4	Concluding remarks	63
2	Unsaturated soil mechanics applied to road materials	65
2.1	Relevant equations	65
2.1.1	Water retention curve	65
2.1.2	Assessment of the hydraulic conductivity based on the water retention curve	66
2.1.3	Flow of water in unsaturated materials	67
2.1.4	Thermal properties of unsaturated materials	67
2.1.5	Heat flow in unsaturated materials	69
2.2	Example 7: Assessment of the water retention curve using the empirical model proposed in the Mechanistic Empiric Pavement Design Guide (MEPDG)	69
2.3	Example 8: Method for calculating the unsaturated hydraulic conductivity based on the water retention curve	71
2.3.1	Limits of integration and sub-intervals	72
2.3.2	Volumetric water content and derivative with respect to suction	73
2.3.3	Denominator of Equation 2.13	73
2.3.4	Numerator of Equation 2.13	75
2.4	Example 9: Simplified calculation of water infiltration	75
2.5	Example 10: Numerical calculation of water flow in unsaturated materials, application to road structures	78
2.5.1	Part A. Numerical solution of the nonlinear partial differential equation describing the flow of water in unsaturated soils using the explicit finite difference method	80

2.5.1.1	Discretization in space	81
2.5.1.2	Discretization in time	82
2.5.1.3	Implementation of the explicit Finite Difference Method	83
2.5.1.4	Boundary conditions	84
2.5.1.5	Initial conditions	86
2.5.2	Part B. Numerical solution using the data of the example	86
2.5.2.1	Water retention curves	87
2.5.2.2	Discretization in space	89
2.5.2.3	Discretization in time	91
2.5.2.4	Boundary and initial conditions	94
2.5.2.5	Simulation	95
2.6	Example 11: Numerical solution of the heat flow in road structures	99
2.6.1	Part A. Numerical solution of the diffusion equation using the implicit finite difference method	100
2.6.1.1	Discretization in space	100
2.6.1.2	Discretization in time	101
2.6.1.3	Implementation of the FDM using the implicit solution	101
2.6.1.4	Boundary conditions	103
2.6.1.5	Initial conditions	105
2.6.2	Part B. Numerical solution using the data of the example	105
2.6.2.1	Thermal conductivity and heat capacity	105
2.6.2.2	Discretization in space	106
2.6.2.3	Discretization in time	107
2.6.2.4	Boundary and initial conditions	108
2.6.2.5	Simulation	108

3 Compaction **113**

3.1	Relevant equations	113
3.1.1	Summary of the equations describing the BBM	113
3.1.2	Effect of cyclic loading	116
3.1.3	Evolution of the water retention curve during compaction	116
3.1.4	A linear packing model for establishing the relationship between grain size distribution and density	116
3.1.4.1	Virtual compacity of binary mixtures	117
3.1.5	Virtual compacity of binary mixtures without interaction	118
3.1.6	Virtual compacity of binary mixtures with total interaction	119
3.1.7	Virtual compacity of binary mixtures with partial interaction	121
3.1.7.1	Virtual compacity of polydisperse mixtures	123
3.1.7.2	Actual compacity of granular mixtures	124
3.1.7.3	Assessment of compacted densities using the linear packing model	126
3.2	Example 12: Simulation of field compaction using the BBM	127
3.2.1	Stress distribution produced by one tire on the surface of the soil	129
3.2.2	Stress distribution within the soil mass	132
3.2.3	Stress distribution produced by the whole compactor	133

3.2.4	Compaction profiles calculated using the BBM	136
3.2.5	Effect of the loading cycles	138
3.2.6	Effect of the water content	141
3.3	Example 13: Use of the linear packing model to compute the density of a compacted material based on its grain size distribution	141
3.3.1	Virtual compacity	142
3.3.2	Actual compacity	143
3.3.3	Dry density	145
3.3.4	Results of the model and comparison with the Proctor test	146
4	Embankments	147
4.1	Relevant equations	147
4.1.1	Stress components due to triangular loads	147
4.1.2	Immediate settlements	147
4.1.3	Primary consolidation	148
4.1.4	Radial consolidation	149
4.1.5	Increase of shear strength for staged construction	149
4.1.6	Generalized bearing capacity	149
4.1.7	The BBM including the effect of soil's microstructure	150
4.2	Example 14: Embankments on soft soils	152
4.2.1	Stress distribution beneath the symmetry axis of the embankment	153
4.2.2	Immediate and consolidation settlements	154
4.2.3	Vertical stress distribution under the embankment for the final height of the fill.	156
4.2.4	Evaluation of the bearing capacity for the staged construction	157
4.2.5	Evaluation of the bidimensional consolidation	161
4.2.6	Evolution of the undrained shear strength considering the 2D consolidation	166
4.2.7	Evaluation of the safety factor before placing each stage	166
4.2.8	Analysis of the radial drainage	168
4.3	Example 15: Analysis of the collapse of embankments under soaking using the BBM	171
4.3.1	Simulation of the oedometric compaction	173
4.3.2	Post compaction	178
4.3.3	Reloading	180
4.3.3.1	Elastic domain	181
4.3.3.2	Elastoplastic domain	183
4.3.4	Soaking	183
4.3.5	Concluding remarks	186
4.4	Example 16: Effect of the soil's microstructure in the collapse of embankments	191
4.4.1	Initial conditions	192
4.4.2	Oedometric compression	193
4.4.2.1	Elastic compression	193
4.4.2.2	Elastoplastic compression	193
4.4.3	Saturated oedometric compression	194

5	Mechanical behavior of road materials	197
5.1	Relevant equations	197
5.1.1	Models describing the resilient modulus	197
5.1.2	Models describing the resilient Young's modulus and Poisson's ratio	198
5.1.3	Effect of water in the resilient Young's modulus	199
5.2	Example 17: Adjustment of the measured resilient Young's modulus using different models	200
5.2.1	Fitting the experimental results using the $k - \theta$ model	201
5.2.2	Fitting the experimental results using the three parameters model	202
5.2.3	Fitting the experimental results using Boyce's model	204
5.2.4	Fitting the experimental results using the linear model	206
5.2.5	Performance of the different models to predict resilient Young's moduli and Poisson's ratios	209
5.3	Example 18: Assessment of the effect of the water content of the granular layer on the fatigue life of a low-traffic road structure	211
5.3.1	Fitting the experimental measures of suction using the van Genuchten equation	213
5.3.2	Evaluation of the models that describe the effect of the water content on the resilient Young's modulus	216
5.3.2.1	Models recommended in the MEPD	216
5.3.2.2	Model with two state variables: vertical total stress and suction	218
5.3.2.3	Model based on effective stress	221
5.3.2.4	Comparison of models' performance	222
5.3.3	Fatigue lifespan of the bituminous layer depending on the water content of the granular layer	224
5.3.4	Concluding remarks	231
6	Climate effects	233
6.1	Relevant equations	233
6.1.1	Heat flow in road structures	233
6.1.2	Flow of water through a drainage layer	236
6.2	Example 19: Evolution of the temperature in a road structure depending on the environmental variables	237
6.2.1	Environmental variables	239
6.2.2	Heat flow due to solar radiation	240
6.2.3	Discretization in space	244
6.2.4	Discretization in time	245
6.2.5	Continuity equation between layers	246
6.2.6	Analysis of the boundary conditions	247
6.2.7	Analysis of the time step	248
6.2.8	Numerical solution	249
6.3	Example 20: Assessment of the local infiltration through cracks in the top layer of a road	254
6.3.1	Infiltration through single cracks	255

6.3.2	Infiltration through a squared net of cracks	257
6.4	Example 21: Drainage layers in road structures	258
7	Nondestructive evaluation and inverse methods	263
7.1	Relevant equations	263
7.1.1	Theoretical analysis of vibratory rollers	263
7.1.2	Contact between a cylindrical body and an elastic half-space	264
7.1.3	The cone macroelement model	265
7.1.4	Continuous compaction control (CCC)	265
7.2	Example 22: Soil–drum interaction assuming an elastic soil’s response	266
7.2.1	Discretization in time of the dynamic equation	266
7.2.2	Effect of Young’s modulus on the soil–drum interaction	269
7.2.3	Effect of the dynamic load	272
7.3	Example 23: Analysis of the soil–drum interaction considering the soil’s reaction into the elastoplastic domain of behavior	276
7.3.1	Contact soil–drum under monotonic loading and elastoplastic behavior	278
7.3.2	Cyclic loading with elastoplastic soil’s response	284
7.3.3	Dynamic soil–drum interaction considering the elastoplastic contact	285
	<i>Bibliography</i>	289
	<i>Index</i>	293

Author Biography

Bernardo Caicedo obtained his undergraduate degree in civil engineering at the Universidad del Cauca in Colombia in 1985. He received the Francisco José de Caldas Medal for his academic achievements, which is only awarded about once in every 10 years. He did his doctoral work at L'Ecole Centrale de Paris in 1991 and is working at the Laboratoire Central des Ponts et Chaussées in Paris.

He joined the “Universidad de los Andes, Uniandes” in Colombia in 1991. He has been involved in teaching, research, and administrative duties here for around 29 years now. During his first period at Uniandes, his research focused on bringing the laboratory to a high standard of international competitiveness. This effort has met with relatively good success. One example of this work was the design and construction, under his leadership, of two geotechnical centrifuges used for teaching and research. One of these machines is equipped with an environmental chamber including leading technologies to simulate climate in experiments using the centrifuge. Other major laboratory apparatus designed and constructed under his direction were a large hollow cylinder apparatus, a linear test track for physical modeling of pavements, and a 60-ton shaking table.

His research activities cover a broad spectrum of areas in geotechnical engineering. They include studies of soil dynamics, unsaturated soils, physical modeling of unsaturated soils (expansive and collapsing soils), study of the behavior of unbound granular materials for pavements, the development of new pavement design methods based on mechanistic concepts with climatic interactions, and the study of the mechanical behavior of multi-phase soils (unsaturated soils) including chemical (chemo-mechanics) and biological aspects. His efforts to develop laboratory facilities have allowed him to publish several documents: to date, he has published more than 200 documents including 2 books, 65 papers in indexed journals, 5 keynote lectures, 89 papers in reviewed international conferences, 12 in other international conferences, and 51 in local conferences. He is a member of the editorial panel of two international journals: *Transportation Geotechnics* (Elsevier) and *Acta Geotechnica*. In addition, he is a member of the board of the TC202 committee (Transportation Geotechnics) and vice chair of the TC 106 committee (Unsaturated Soils) of the International Society of Soil Mechanics and Geotechnical Engineering ISSMGE.

He has received several awards from the Institution of Civil Engineers (ICE): the Telford Premium in 2016, the Geotechnical Research Medal in 2018, and the Mokshagundam Visvesvaraya Award in 2020.



Taylor & Francis

Taylor & Francis Group

<http://taylorandfrancis.com>

Acknowledgments

This book is the result of two years of work, and it was finalized during the pandemic of 2019–2020. For me, it is a pleasure to acknowledge the people who made it possible.

First of all, I would like to express my gratitude to my wife Gloria and my sons Alejandro and Nicolas. They encourage me in all moments and also provide me an environment of happiness that makes all the big projects possible.

A significant recognition is due to the University of Los Andes and its Department of Civil and Environmental Engineering which supported this work. Special gratitude goes to my colleagues from our Geomaterials and Infrastructure Systems research group: Silvia Caro, Laura Ibagón, Julieth Monroy, Mauricio Sánchez, Nicolás Estrada, Miguel Angel Cabrera, and to my colleagues and friends in the Department.

Research in geotechnical engineering has given me the pleasure of finding a community of friends and bright people; this book would not have been possible without the knowledge and friendship they have offered me.

I would express my gratitude to some graduate students who helped me in reviewing some of the examples and MATLAB[®] scripts: Carlos Vladimir Benavides, Lina María Pua, Juan Villacreses, Jorge Mario Lozano, and many others that I had the privilege to advise in the last 30 years.



Taylor & Francis

Taylor & Francis Group

<http://taylorandfrancis.com>

List of mathematical symbols

The following table presents the list of the main mathematical symbols used throughout the book. However, it is important to remark that sometimes the same symbol has several meanings. For this reason, the reader must verify the context and the definition of the symbols presented below each equation.

ROMAN LETTERS

Symbol	Definition
A_i	Constant for the Burmister's method.
A_{σ_v}	Slope relating the Young's modulus and the vertical stress.
A_{ω}	Amplitude of the fundamental frequency of a vibratory drum compactor.
$A_{2\omega}$	Amplitude of the first harmonic of a vibratory drum compactor.
a	Radius of a circular loaded area, or half axis of a super elliptical contact area, or half contact width for the Hertz contact theory, or parameter of the water retention curve.
$a_{i,j}$	Decompaction coefficient of a granular mixture.
B_i	Constant for the Burmister's method.
b	Half axis of a super elliptical contact area, or intermediate principal stress parameter.
$b_{j,i}$	Wall coefficient of a granular mixture.
C_{AK}	Proportionality factor for defining the contact stress between a tire and the road.
C_c	Compression coefficient measured in oedometric compression tests.
C_i	Constant for the Burmister's method.
C_r	Recompression coefficient.
C_s	Coefficient of the dashpot representing the soil below a drum compactor.
C_{θ}	Specific water capacity.
CMV	Compaction meter value.
c	Dashpot constant.
c_H	Specific heat capacity.
c_{H_v}	Volumetric heat capacity of the soil.
c_h	Coefficient of horizontal consolidation.
c_s	Specific heat of the solid grains.

(Continued)

Symbol	Definition
c_u	Undrained shear strength in saturated state.
c_v	Coefficient of vertical consolidation.
c_w	Specific heat of water.
c_1	Damping coefficient of the tire for defining the truck-road interaction.
c_2	Damping coefficient of the suspension's shock absorber for defining the truck-road interaction.
D_{hg}	Time difference between the time of a site and the time zone's reference point.
D_i	Constant for the Burmister's solution.
d_n	Julian day.
d_x	Size of the sieve corresponding to $x\%$ by weight of those which passed through the sieve.
d_{60}	Grain size corresponding to 60 % by mass of those that passed through this dimension.
E	Young's modulus.
E^*	Equivalent Young's modulus.
E_r	Resilient Young's modulus.
E_{r-opt}	Resilient modulus at optimum moisture content
E_u	Undrained Young's Modulus
E_0	Correction factor for the direct radiation.
$E_{0\sigma_v}$	Young's resilient modulus for zero vertical stress.
e	Void's ratio, or eccentricity of the mass of a vibratory drum.
e_m	Microstructural void's ratio for the microstructural BBM.
e_0	Initial void's ratio for computing settlements due to consolidation.
$f(t)$	Vector that represents the road profile as a time signal.
G	Shear modulus.
G_a	Fitting coefficient of the Boyce's model.
G_r	Resilient shear modulus.
g	Acceleration of the gravity.
H	Normalized thickness of the road structure.
h	Angle between the center of the disc of the sun and the horizon, the solar zenith angle.
h_c	Convection coefficient
I	Irradiance
I_b	Direct irradiance.
I_d	diffuse irradiance.
I_0	Solar constant.
J_0	Bessel function of the first kind and order zero.
J_1	Bessel function of the first kind and order one.
K	Coefficient of volumetric compressibility, or packing coefficient of a granular mixture.
K_a	Fitting coefficient of the Boyce's model.
K_e	Kersten's number.
K_i	Coefficient that relates the packing state of grains i within a granular mixture.

(Continued)

Symbol	Definition
K_N	Coefficient relating the increase in density depending on the loading cycles.
K_r	Resilient coefficient of volumetric compressibility.
k_c	Parameter of the BBM model relating the increase in tensile strength due to an increase of suction.
k_H	Thermal conductivity.
k_{Hi}	Thermal conductivity of ice.
k_{Hs}	Thermal conductivity of the solid grains.
k_{Hw}	Thermal conductivity of water.
k_s	Slope of the unloading-reloading curve in the space relating matric suction to the degree of saturation.
k_s^e	Coefficient of the spring representing the soil below a drum compactor.
k_w	Hydraulic conductivity.
k_1	Fitting coefficient to model the resilient Young's modulus, or spring constant of a tire for defining the truck-road interaction.
k_2	Fitting coefficient to model the resilient Young's modulus, or spring constant of the suspension for defining the truck-road interaction.
k_3	Fitting coefficient to model the resilient Young's modulus.
$l_T(y)$	Length of the contact area between a tire and the road.
M	Slope of the critical state line in the p q plane.
m	Mass, or parameter of the water retention curve, or $m = 1/v$.
m_d	Mass of a vibratory drum.
m_e	Eccentric mass of a vibratory drum.
m_f	Mass of the frame of a vibratory drum
m_W	Parameters of the water retention model that depends on void's ratio.
m_1	Mass of the axle for defining the truck-road interaction.
m_2	Mass of the body of the vehicle for defining the truck-road interaction.
$N(s)$	Specific volume in unsaturated state for a mean net stress of p^c .
$N(0)$	Specific volume in saturated state for a mean net stress of p^c .
n	Porosity, or exponent representing the rectangularity of a super elliptical contact area, or parameter of the water retention curve, or fitting coefficient of the Boyce's model.
n_c	Number of grain classes in a granular mixture.
n_{sm}	Smoothing parameter of the function representing the effective degree of saturation.
n_W	Parameters of the water retention model that depends on void's ratio.
P_{200}	Proportion of material that pass through the # 200 U.S. Standard Sieve.
PI	Plasticity Index.
p	Mean stress.
\bar{p}	Constitutive mean stress for the microstructural BBM.
p_a, p_{atm}	Atmospheric pressure.
p_c	Cyclic mean stress.
p^c	Reference stress for the BBM.
\bar{p}_c	Reference mean constitutive stress for the microstructural BBM.

(Continued)

Symbol	Definition
p_0	Maximum stress at for the Hertz contact theory.
p_0^*	Over consolidation mean stress in the saturated state.
q	Deviator stress, or uniform load over a circular loaded area.
q_c	Cyclic deviator stress.
q_{conv}	Heat flux due to convection.
q_{rad}	Heat flux due to radiation.
q_{sens}	Sensible heat flux.
q_{th}	Heat flux due to thermal emissions
R	Radial distance $R = \sqrt{x^2 + y^2 + z^2}$.
R_e	Reynolds number.
RMV	Resonant meter value.
r	Constant of the BBM relating maximum stiffness at infinite.
\bar{r}	Material parameter for the microstructural BBM.
S_r	Degree of saturation.
\bar{S}_r	Effective degree of saturation for the microstructural BBM.
S_{r-opt}	Degree of saturation at the optimum water content.
S_{r0}	Degree of saturation at the beginning of unloading.
$S_z(\Omega)$	Power Spectral Density, PSD, of the road's profile.
s	Matric suction.
s_{aev}	Suction corresponding to the air entry value.
s_b	Air entry suction.
s_{res}	Residual suction.
s_0	Suction at the beginning of unloading.
\bar{s}_λ	Material parameter for the microstructural BBM.
T	Temperature.
T_a	Air temperature.
T_d	Dew point temperature.
T_l	Local time in the zone of a particular site.
T_s	Temperature at the surface of the road.
T_{sv}	True solar time at a particular site.
T_{sky}	Hypothetical temperature above the surface of the road.
T_v	Time factor for vertical consolidation.
t	Time.
$U(t)$	Degree of consolidation achieved at time t .
$U_v(t)$	Degree of vertical consolidation.
U_{vr}	Degree of consolidation in the radial and vertical directions.
U_w	Relative humidity.
\mathbf{u}	Vector representing the displacements of the axle and the body of a vehicle.
u	Displacement towards the x axis.
u_a	Pore air pressure.
u_g	Function for defining the road's profile.
u_v	Vapor pressure.
u_{vs}	Saturation vapor pressure.
u_w	Pore water pressure.
\bar{u}_{wce}	Average excess pore water pressure.

(Continued)

Symbol	Definition
V_a	Air velocity.
v	Displacement towards the y axis, or Specific volume ($v = 1 + e$).
w	Gravimetric water content, or displacement towards the z axis, or hour angle indicating the position of the sun in a day, or waviness index for defining the road's profile.
$w_T(x)$	Width of the contact area between a tire and the road
x	Cartesian coordinate.
y	Cartesian coordinate.
y_i	Volumetric proportion of grains in a granular mixture.
Z_n	Amplitude of the n^{th} harmonic for defining the road's profile.
z	Cartesian coordinate.
z_s	Soil displacement below a drum compactor.

GREEK LETTERS

Symbol	Definition
α	Mean absorptivity coefficient, or normalized radius of a circular loaded area.
α_K	Parameter describing the contact stress between a tire and the road.
β	Parameter of the BBM giving the shape of the function for the increase of stiffness due to an increase of suction, or angle to define the point where the stress is calculated using the Fröhlich's solution, or coefficient of the Boyce's model.
$\bar{\beta}$	Material parameter of the microstructural BBM.
β_i	Residual compacity of grains i in a granular mixture.
Γ	Angle indicating the position of the earth in its orbit for a particular day of the year.
γ	Unit weight, or virtual compacity of a granular mixture.
ΔT_l	Time difference between the local time and the standard time.
$\Delta\Omega$	Width of each frequency band for defining the road's profile.
δ	Solar declination.
δ_K	Parameter describing the contact stress between a tire and the road.
ϵ	Emissivity coefficient.
ϵ_v	Volumetric strain.
ϵ_1, ϵ_2	Geometrical variables to define a triangular load over a half space.
η	Empirical parameter for computing the thermal conductivity of soils.
θ	Volumetric water content, or bulk stress, or Angle between a normal vector on the surface of the road and a direct line joining the sun.
θ_i	Volumetric fraction of ice in a soil.

(Continued)

Symbol	Definition
θ_{res}	Residual volumetric water content.
θ_s	Volumetric fraction of the solid grains in a soil.
$\theta'(s)$	First derivative of the water retention curve.
θ_{sat}	Saturated volumetric water content.
θ_w	Volumetric fraction of water in a soil.
κ	Road's roughness coefficient for defining the road's profile, or slope of the overconsolidated domain, in logarithmic scale, of the compression line in the saturated state.
κ_H	Empirical parameter for computing the thermal conductivity of soils.
κ_s	Parameter of the BBM relating the change in specific volume due to an increase of matric suction.
λ	Normalized depth for the Burmister's solution, or slope of the virgin compression line in the saturated state.
$\bar{\lambda}$	Compressibility coefficient for the microstructural BBM.
$\lambda(0)$	Slope, in logarithmic scale, of the compression line in the saturated state.
$\lambda(s)$	Slope, in logarithmic scale, of the compression lines in the unsaturated state
$\bar{\lambda}(\bar{s})$	Coefficient of compressibility depending on the effective suction.
ν	Poisson's ratio.
ξ	Fröhlich's concentration factor.
ξ_m	Variable describing the microstructural state of a soil.
ρ	Radial distance in the cylindrical coordinate system.
ρ_c	Settlement due to primary consolidation.
ρ_d	Dry density.
ρ_H	Normalized radial distance used in Burmister's solution.
ρ_i	Immediate settlement.
ρ_w	Density of water.
σ	Total stress, or Stefan-Boltzmann constant.
σ'_c	Over consolidation effective stress for computing settlements due to consolidation.
σ_{net}	Net stress.
σ_{oct}	Octahedral stress.
σ_{u_g}	Standard deviation of the ISO road's profile.
$\sigma'_{u'_g}$	Standard deviation of the first derivative of the ISO road's profile.
σ_v	Vertical stress.
$\sigma_{v_{N_C}}$	Vertical stress required to reach a specific density by applying N_C loading cycles.
$\sigma_{v_{N_C=1}}$	Vertical stress required to reach a particular density when applying one loading cycle.
$\sigma_x, \sigma_y, \sigma_z$	Normal stresses in the Cartesian coordinate system.
σ'_{z0}	Initial effective vertical stress for computing settlements due to consolidation.
$\sigma_1, \sigma_2, \sigma_3$	Principal stresses.
τ_{oct}	Octahedral shear stress.
Φ	Compacity of a granular mixture.
Φ_i	Partial volume of class i in a granular mixture.

(Continued)

Symbol	Definition
ϕ	Latitude on the earth of a particular site.
ϕ'	Friction angle in effective stresses.
ϕ_n	Phase angle of the n^{th} harmonic for defining a road's profile.
ϕ_W	Parameters of the water retention model that depends on the void's ratio.
χ	Effective stress parameter.
χ_H	Empirical parameter for computing the thermal conductivity of soils.
ψ	Water potential.
ψ_W	Parameters of the water retention model that depends on the void's ratio.
Ω	Angular frequency.
Ω_L	Lower limit for the spatial reference frequency to define a road's profile.
Ω_n	Central frequency of the n^{th} band to define a road's profile.
Ω_U	Upper limit of the spatial reference frequency to define a road's profile.
Ω_0	Spatial reference frequency to define a road's profile.
ω	Angular frequency, or angle to define the point where the stress is calculated using the Fröhlich's solution.



Taylor & Francis

Taylor & Francis Group

<http://taylorandfrancis.com>

Introduction

This book develops 23 extended examples that cover most of the theoretical aspects presented in the book *Geotechnics of Roads, Fundamentals*, [10]. Moreover, for most examples, this book describes algorithms for solving complex problems and provides MATLAB scripts for their solution. Consequently, this book is a natural complement of the book *Geotechnics of Roads, Fundamentals*.

Although most of the theories required to solve the examples were described in detail in [10], each chapter in this book summarizes the set of equations required to solve the examples. This book has seven chapters as follows:

Chapter 1 of this book deals with the distribution of stresses and strains in road structures. It develops six examples that cover, first, the analysis of the stresses and displacements produced by vertical or horizontal loads in elastic half-spaces. Then, it describes the analysis of the tire–road interaction using Hertz’s theory and the Fröhlich stress distribution. Besides, the chapter describes in detail the use of Burmister’s method to calculate the stress distribution in structures of multilayered roads. Concerning elastodynamic solutions, this chapter presents an example that describes the calculation of the vehicle–road interaction that produces dynamic loads on the road. These loads could exceed the static load obtained by forgetting the dynamic interaction.

Chapter 2 deals with the unsaturated soil mechanics applied to road structures. It describes the methodology to assess the water retention curve using the empirical model proposed in the Mechanistic Empiric Pavement Design Guide (MEPDG). Then, it presents the method for calculating the unsaturated hydraulic conductivity based on the water retention curve. Moreover, regarding the flow of water in road structures, the chapter describes a simplified calculation of water infiltration. Then, it presents a more rigorous methodology based on the numerical calculation of water flow in unsaturated materials. Finally, regarding heat flow, the chapter presents an example describing the methodology for the numerical calculation of the evolution of temperature in road structures.

Chapter 3 analyzes soil compaction through two examples. The first one focuses on the compaction process interpreted as a hardening process of unsaturated soils. Therefore, this example uses the elastoplastic model Barcelona Basic Model (BBM) to analyze the evolution of irreversible volumetric strains within the soil produced by a tire compactor. The chapter also explains a linear packing model that allows assessing the density of compacted materials based on its grain size distribution, the second example of this chapter uses this methodology to compute the maximum density of Proctor’s tests.

Chapter 4 develops three examples regarding the construction and the performance of embankments. The first example deals with the construction of embankments on soft soils; it explains in detail the use of the methodology of staged construction to design

an embankment that has a proper safety factor and also analyzes the magnitude of settlement to estimate the correct height of the fill. The second and third examples analyze the collapse of embankments and link the compaction characteristics with the long-term deformation of embankments subject to wetting. For this purpose, these examples use the theory of unsaturated soil mechanics and the elastoplastic BBM. Such examples consider or not the effect of soil's microstructure.

Chapter 5 explains the essential subject of the mechanical behavior of road materials. Methodologies explained in this chapter are crucial to use mechanistic approaches that allow consideration of different load and climatic conditions that can affect roads. Two examples illustrate this effect; the first one explains the methodologies to adjust the laboratory measurements of the resilient Young's modulus to the different models that allow a mathematical description of its evolution regarding stresses, water content, or matric suction. The second example of this chapter uses the change of the resilient Young's modulus depending on the matric suction to assess the effect of the water content of the granular layer on the fatigue life of a low traffic road structure.

Chapter 6 is devoted to the climate effects on road structures. The chapter develops three examples. The first one explains the process to compute the evolution of the temperature in a road structure along a day of the year; the analysis includes several climatic variables such as the solar radiation, the air temperature, the wind velocity, the relative humidity, the latitude of the site, and the day of the year. Moreover, this chapter develops two other examples regarding the flow of water, one of them analyzes the effect of the cracks of the bituminous layer in the infiltration of water toward the road structure, and the second one analyses the capacity of a drainage layer to evacuate the infiltrations of water.

Finally, **Chapter 7** explains the theoretical tools that allow analyzing the performance of vibratory compactors and the procedure to examine their movement to apply the methodology of continuous compaction control. The chapter presents two examples; the first one considers the layer under compaction as an elastic material, while the second considers the elastoplastic response of the material undergoing compaction.

Distribution of stresses and strains in roads

I.1 RELEVANT EQUATIONS

The performance of road structures results from the interaction between the stress produced by the external loads and the behavior of the different constituent materials. Also, since roads must undergo thousands to millions of load repetitions, their constituent materials must sustain loads without suffering irreversible strains. Therefore, they must remain in the elastic domain of behavior.

This chapter focuses on the calculation of stresses in road structures. First, it describes methodologies that allow calculating the stress distribution produced by vertical and horizontal loads in a homogeneous half-space. Then, the chapter describes a methodology for calculating road loads due to interaction with vehicles. Finally, the chapter describes Burmister’s method, which is the usual method to calculate stresses and strains in road structures having multiple layers.

I.1.1 Boussinesq’s solution

In 1878, Boussinesq proposed a solution that allows calculating the distribution of stresses in a half-space beneath a concentrated load [6]. The set of equations that permit to obtain the stress components resulting from a concentrated vertical load P located in the Cartesian coordinate system, as indicated in Figure 1.1, are

$$\sigma_x = \frac{3P}{2\pi} \left\{ \frac{x^2 z}{R^5} - \frac{m-2}{3m} \left[-\frac{1}{R(R+z)} + \frac{(2R+z)x^2}{(R+z)^2 R^3} + \frac{z}{R^3} \right] \right\}, \quad (1.1)$$

$$\sigma_y = \frac{3P}{2\pi} \left\{ \frac{y^2 z}{R^5} - \frac{m-2}{3m} \left[-\frac{1}{R(R+z)} + \frac{(2R+z)y^2}{(R+z)^2 R^3} + \frac{z}{R^3} \right] \right\}, \quad (1.2)$$

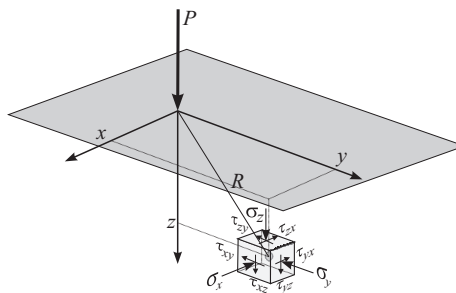


Figure 1.1 Geometric layout to describe the Boussinesq solution in Cartesian coordinates.

$$\sigma_z = \frac{3P}{2\pi} \frac{z^3}{R^5}, \quad (1.3)$$

$$\tau_{xy} = \frac{3P}{2\pi} \left\{ \frac{xyz}{R^5} - \frac{m-2}{3m} \left[\frac{(2R+z)xy}{(R+z)^2 R^3} \right] \right\}, \quad (1.4)$$

$$\tau_{yz} = \frac{3P}{2\pi} \frac{yz^2}{R^5}, \quad (1.5)$$

$$\tau_{zx} = \frac{3P}{2\pi} \frac{xz^2}{R^5}, \quad (1.6)$$

where x , y , z are the Cartesian coordinates, $R = \sqrt{x^2 + y^2 + z^2}$, $m = 1/\nu$, and ν is Poisson's ratio.

Also, the expressions that provide the horizontal displacements u and v , and the vertical displacement w are

$$u = \frac{1+\nu}{2\pi E} \left[\frac{xz}{R^3} - \frac{(1-2\nu)x}{R(R+z)} \right] P, \quad (1.7)$$

$$v = \frac{1+\nu}{2\pi E} \left[\frac{yz}{R^3} - \frac{(1-2\nu)y}{R(R+z)} \right] P, \quad (1.8)$$

$$w = \frac{1+\nu}{2\pi E} \left[\frac{z^2}{R^3} + \frac{2(1-\nu)}{R} \right] P, \quad (1.9)$$

where E is Young's modulus.

1.1.2 Cerruti's solution

Shortly after Boussinesq, in 1882, Cerruti proposed a set of expressions for calculating the stress distribution in half-space beneath a horizontal load [16]. His solution provides the following expressions for the stresses' distribution produced by a concentrated horizontal load H located in the Cartesian plane as depicted in Figure 1.2:

$$\sigma_x = -\frac{Hx}{2\pi R^3} \left\{ -\frac{3x^2}{R^2} + \frac{1-2\nu}{(R+z)^2} \left[R^2 - y^2 - \frac{2Ry^2}{R+z} \right] \right\}, \quad (1.10)$$

$$\sigma_y = -\frac{Hy}{2\pi R^3} \left\{ -\frac{3y^2}{R^2} + \frac{1-2\nu}{(R+z)^2} \left[3R^2 - x^2 - \frac{2Rx^2}{R+z} \right] \right\}, \quad (1.11)$$

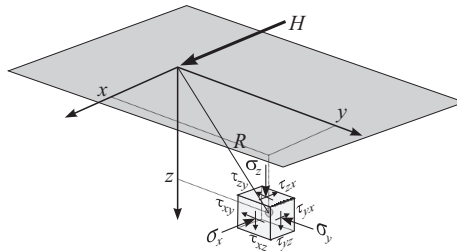


Figure 1.2 Geometric layout to describe the Cerruti solution in Cartesian coordinates.

$$\sigma_z = \frac{3Hxz^2}{2\pi R^5} \quad (1.12)$$

$$\tau_{xy} = -\frac{Hy}{2\pi R^3} \left\{ -\frac{3x^2}{R^2} + \frac{1-2\nu}{(R+z)^2} \left[-R^2 + x^2 + \frac{2Rx^2}{R+z} \right] \right\}, \quad (1.13)$$

$$\tau_{yz} = \frac{3Hxyz}{2\pi R^5}, \quad (1.14)$$

$$\tau_{zx} = \frac{3Hx^2z}{2\pi R^5}, \quad (1.15)$$

Also, x , y , z are the Cartesian coordinates, and $R = \sqrt{x^2 + y^2 + z^2}$.

Moreover, the displacements u , v , and w provided by Cerruti's solution are

$$u = \frac{H}{4\pi GR} \left\{ 1 + \frac{x^2}{R^2} + (1-2\nu) \left[\frac{R}{R+z} - \frac{x^2}{(R+z)^2} \right] \right\}, \quad (1.16)$$

$$v = \frac{H}{4\pi GR} \left\{ \frac{xy}{R^2} - (1-2\nu) \frac{xy}{(R+z)^2} \right\}, \quad (1.17)$$

$$w = \frac{H}{4\pi GR} \left\{ \frac{xz}{R^2} + (1-2\nu) \frac{x}{R+z} \right\}, \quad (1.18)$$

where G is the shear modulus, and ν is Poisson's ratio.

1.1.3 Fröhlich solution

Fröhlich [32] introduced a "concentration factor", ξ , into Boussinesq's equations. The Fröhlich solution is a rough alternative to account for the modification of the stress distribution due to plasticity. However, Fröhlich's solution is not exact because it respects the equilibrium conditions but without considering the equations for displacement's compatibility. Despite the approximation of the Fröhlich solution, it produces good agreement with the measures of field stresses, mainly when a layer of soil undergoes compaction [40].

Equation 1.19 gives Fröhlich's solution for the radial stress produced by a combination of vertical and horizontal point loads (P , H) [39,41].

$$\sigma_R = \frac{\xi P}{2\pi R^2} \cos^{\xi-2} \beta + (\xi - 2) \frac{\xi H}{2\pi R^2} \cos \omega \sin \beta \cos^{\xi-3} \beta, \quad (1.19)$$

$$\sigma_\theta = 0. \quad (1.20)$$

In Equation 1.19, β is the angle formed by the vertical axis and a vector joining the point where the load is applied and the point where the stress is calculated. At the same time, ω is the angle between the horizontal load vector and a vertical plane including the vector mentioned above (in other words, the plane Ω represented in Figure 1.3).

In Cartesian coordinates, Equations 1.19 and 1.20 lead to the following stresses:

$$\sigma_x = \sigma_R \sin^2 \beta \cos^2 \omega = \sigma_R \frac{x^2}{R^2}, \quad (1.21)$$

$$\sigma_y = \sigma_R \sin^2 \beta \sin^2 \omega = \sigma_R \frac{y^2}{R^2}, \quad (1.22)$$

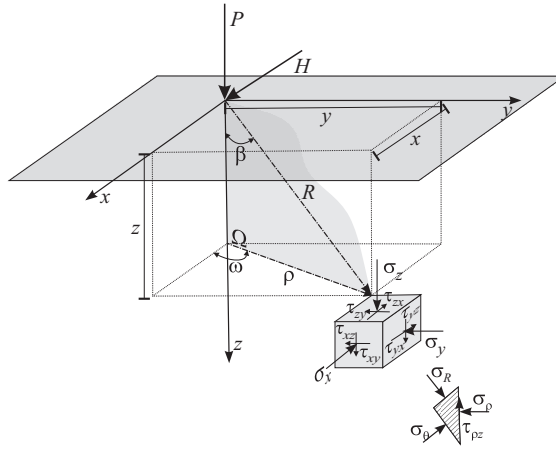


Figure 1.3 Geometric layout to describe the Fröhlich solution in Cartesian coordinates. (Adapted from Ref. [39].)

$$\sigma_z = \sigma_R \cos^2 \beta = \sigma_R \frac{z^2}{R^2} \quad (1.23)$$

$$\tau_{xy} = \sigma_R \sin^2 \beta \cos \omega \sin \omega = \sigma_R \frac{xy}{R^2}, \quad (1.24)$$

$$\tau_{xz} = \sigma_R \cos \beta \sin \beta \cos^2 \omega = \sigma_R \frac{xz}{R^2}, \quad (1.25)$$

$$\tau_{yz} = \sigma_R \cos \beta \sin \beta \sin^2 \omega = \sigma_R \frac{yz}{R^2}. \quad (1.26)$$

1.1.4 Tire–soil interaction

The contact area of the footprint below a tire can be approximated by a superellipse represented by Equation 1.27 as first suggested in Ref. [40]:

$$\left| \frac{x}{a} \right|^n + \left| \frac{y}{b} \right|^n = 1, \quad (1.27)$$

where a and b are the half axes of the super-ellipse, and n is an exponent representing its rectangularity.

Then, the footprint area is limited by Equation 1.28:

$$\Omega = \{(x, y) (|x/a|^n + |y/b|^n \leq 1)\}. \quad (1.28)$$

Equation 1.29 provides a stress distribution function accounting for different tires, which was proposed in Ref. [40]. From this equation, the transverse and longitudinal distributions of vertical stress over the loaded area are

$$\begin{aligned} \sigma_z(x=0, y) &= C_{AK} \left(0.5 - \frac{y}{w_T(x)} \right) e^{-\delta_K(0.5-y/w_T(x))} \quad \text{for } 0 \leq y \leq \frac{w_T(x)}{2}, \quad \text{and} \\ \sigma_z(x, y) &= \sigma_z(x=0, y) \left[1 - \left(\frac{x}{l_T(y)/2} \right)^{\alpha_K} \right] \quad \text{for } 0 \leq x \leq \frac{l_T(y)}{2}, \quad (1.29) \end{aligned}$$

where $w_T(x)$ and $l_T(y)$ are the width and the length of the contact area, δ_K and α_K are parameters given in Ref. [40] that depend on the tire characteristics, and C_{AK} is a proportionality factor that accounts for the total load of the tire.

Another possibility allowing an approximate evaluation of the interaction tire–soil is to use of the Hertz contact theory. This procedure is explained in Example 3.

1.1.5 Road–vehicle interaction

Roads generally have a certain roughness of different wavelengths; at the same time, vehicles, which can be described as a dynamic system, interact with the roughness of the road. This interaction produces a dynamic load on the road whose magnitude depends on the speed of the vehicle, its dynamic characteristics, and the roughness of the road.

The ‘quarter car model’ permits to schematize the road–vehicle interactions. It describes the vehicle, with its tire and suspension, as a set of masses and springs, as shown in Figure 1.4.

The movement of the components of the quarter car is represented by the following second-order linear differential equation with two degrees of freedom [65]:

$$M\ddot{\mathbf{u}} + C\dot{\mathbf{u}} + K\mathbf{u} = \mathbf{f}(t), \quad (1.30)$$

where $\mathbf{u} = [u_1, u_2]^T$ is the vector representing the displacements of the axle and the body of the vehicle, positive in the downward direction, while the mass, damping, and stiffness matrices of the system are

$$M = \begin{bmatrix} m_1 & 0 \\ 0 & m_2 \end{bmatrix}, \quad C = \begin{bmatrix} c_1 + c_2 & -c_2 \\ -c_2 & c_2 \end{bmatrix}, \quad K = \begin{bmatrix} k_1 + k_2 & -k_2 \\ -k_2 & k_2 \end{bmatrix}, \quad (1.31)$$

where k_1 is the spring constant of the tire, k_2 is the spring constant of the suspension, m_1 is the mass of the axle, m_2 is the mass of the body of the vehicle, c_1 is the damping of the tire, and c_2 is the constant of the suspension’s shock absorber.

The road’s profile, described by the function u_g , is positive in the downward direction. The vector that represents the road profile as a time signal $\mathbf{f}(t)$ is

$$\mathbf{f}(t) = \begin{bmatrix} k_1 u_g(t) + c_1 \dot{u}_g(t) + m_1 g \\ m_2 g \end{bmatrix}. \quad (1.32)$$

A methodology for the numerical solution of Equation 1.30 is described in Example 4.

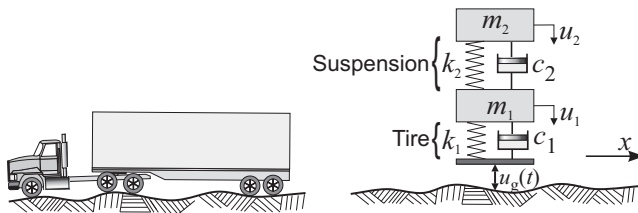


Figure 1.4 Quarter car model to analyze vehicle–road interaction.

1.1.5.1 Mathematical description of road profiles

Based on field data, the standard ISO 8608 [29] proposes to describe the profile of a road in the form of power spectral density (PSD). From Refs. [25,26], the spectral equation that describes the path profile of a single track is

$$S_z(\Omega) = \kappa \left(\frac{\Omega_0}{\Omega} \right)^w, \quad (1.33)$$

$$w = 2 \text{ for } \Omega_L \leq \Omega \leq \Omega_0, \text{ or}$$

$$w = 1.5 \text{ for } \Omega_o \leq \Omega \leq \Omega_U,$$

where $S_z(\Omega)$ is the PSD of the road profile, whose unit is ‘m³/cycle’; the frequencies $\Omega_0 = 1/2\pi$, $\Omega_L = 0.01$, and $\Omega_U = 10$, all in cycles/m, are the spatial reference frequency, and the respective lower and upper limits for frequency; κ is the road roughness coefficient in m³/cycle and w is the waviness index.

In addition, ISO has proposed a road classification system having the seven classes of roughness shown in Table 1.1, and the geometric mean of the coefficient of road roughness κ can be assessed as $\kappa = 4^R \cdot 10^{-6}$.

A particular road profile, described by its power spectrum, can be obtained using the method of superposition of harmonics (SOH) proposed in Refs. [52,53]. The method divides the power spectrum into N frequency bands, each band corresponding to one harmonic. The superposition equation proposed in Ref. [25] is

$$u_g(x) = \sum_{n=1}^N Z_n \sin(2\pi \Omega_n x + \phi_n), \quad n = 1, 2, 3, \dots, N, \quad (1.34)$$

where $u_g(x)$ is the elevation of road profile, x is the forward distance traveled by the vehicle, Z_n is the amplitude of the n^{th} harmonic, $N = (\Omega_U - \Omega_L)/\Delta\Omega$ is the number of frequency bands into which the total PSD spectrum is divided, $\Delta\Omega$ is the width of each frequency band, and ϕ_n is the phase angle of the n^{th} harmonic, which is assumed randomly using a uniform distribution in the interval $[0, 2\pi]$.

The discretization of the PSD leads to the following expression for the central frequency of the n^{th} band:

$$\Omega_n = \omega_L + \frac{2n-1}{2} \Delta\Omega. \quad (1.35)$$

Table 1.1 ISO ranking of road profiles using a Roughness coefficient κ

Road Class	R	$\kappa \cdot 10^6 \text{ m}^3/\text{Cycle}$	
		Range	Geometric Mean
A (very good)	1	<8	4
B (good)	2	8–32	16
C (average)	3	32–128	64
D (poor)	4	128–512	256
E (very poor)	5	512–2,048	1,024
F	6	2,048–8,192	4,096
G	7	8,192–32,768	16,384